APPENDIX B. In-vitro Measurement of the Effective Heat Transfer Coefficient

To ascertain the evaporation rate through the protective tear-film lipid-layer, $\beta \hat{J}_W$, from the heat-transfer model of Eqs. 2 and A8, the effective heat transfer coefficient must be quantified. Because natural convection and radiation occur in parallel, h_{eff} is the sum of h_{nat} and h_{rad}. Both coefficients are requisite.

Radiative heat loss from the ocular surface to the environment obeys the 4th-power temperature-difference law of Stefan-Boltzmann.[46,49] Since the difference between T_S and T_∞ is small relative to absolute environment temperature, the Stefan-Boltzmann equation may be linearized justifying summation of radiative and natural-convective heat transfer coefficients. Linearization also defines $h_{rad} = 4\varepsilon\sigma T_\infty^3$ where ε is the emissivity of water and σ is the Stefan-Boltzmann constant. For environment temperatures close to ambient (T_∞ = 298 K), $h_{rad} \approx 6$ W/m^2/K, and is, therefore, significant compared to those typical natural-convection heat transfer coefficients (i.e., $0.5 \le h_{nat} \le 20$ W/m^2/K).[46,50] Radiation cannot be neglected in environmental cooling of the human eye.

Next, to establish h_{nat} and to validate use of infrared thermography in measuring water evaporation rates, water evaporation rates under conditions of natural convection were determined experimentally, guided by known correlations for heat and mass transfer coefficients.[50] Figure B1 illustrates the apparatus. Evaporation rates of pure water from a small cylindrical vessel were determined under conditions of natural convection using simultaneous infrared thermography and gravimetric analysis. Evaporation of human tear occurs from a vertical orientation, whereas water evaporation in our *in-vitro* experimental apparatus occurs

from a horizontal position. Fortunately, natural-convection mass transfer from a vertical or a horizontal plate differ only slightly.[50]

Water was first heated in a separate 1-L glass beaker to three initial temperatures of roughly 30 ºC, 40 ºC, and 50 ºC and transferred to an insulated, Plexiglas cylindrical container (diameter = 56 mm; height = 10 mm). The Plexiglas vessel was filled to the brim and placed on a zeroed analytical balance (MS 304S, Mettler-Toledo, Columbus, OH). An infrared camera (FLIR A655sc, FLIR Systems) was mounted on a tripod and positioned above the balance, as illustrated in Figure B1. Validity of the IR camera was confirmed before each temperature history by a calibrated iron-constantan thermocouple. Side doors to the balance were kept slightly ajar to prevent humidity buildup and to isolate the balance interior from external air flow. A humidity capacitance probe (Sensirion SHT75 sensor, Zurich, Switzerland) was positioned 5 cm above the water surface to report humidity versus time. For small side-door openings, ambient humidity inside the balance remained constant at 35%.

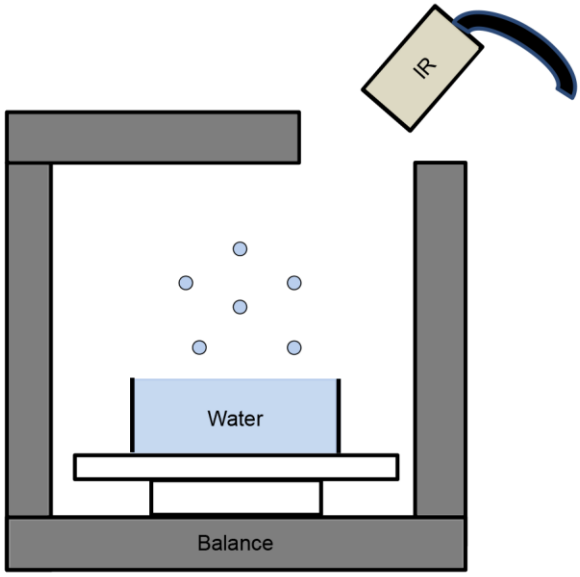

Figure B1. Schematic of the *in-vitro* experimental apparatus to determine the natural convection heat transfer coefficient h_{nat}. An IR camera measures surface temperature versus time as water undergoes evaporative and environmental cooling. Mass loss is determined simultaneously. Not depicted are the opened side doors to the electronic balance.

Water surface temperature versus time was then recorded by the IR camera and mass readings were recorded at 10-min intervals for each initial temperature. Ambient room temperature and relative humidity were recorded for each experiment. Figures B2 and B3 give measured results for the surface-temperature and mass declines. Figure B2 depicts surface temperature as a function of time for water heated to three different initial temperatures (filled symbols). In all cases, water-surface temperature decreases nonlinearly in time. Water at higher temperatures exhibits greater nonlinearity and a larger overall change in temperature over the interval of experiment compared to water at lower temperatures. Figure B3 displays the corresponding transient mass loss for the same three temperatures as in Figure B2 (filled symbols). In all cases, mass decreases with time. Higher temperatures of water correspond to greater rates of mass loss. Importantly, mass loss decreases nonlinearly in time demanding a decreasing water evaporation rate over time.

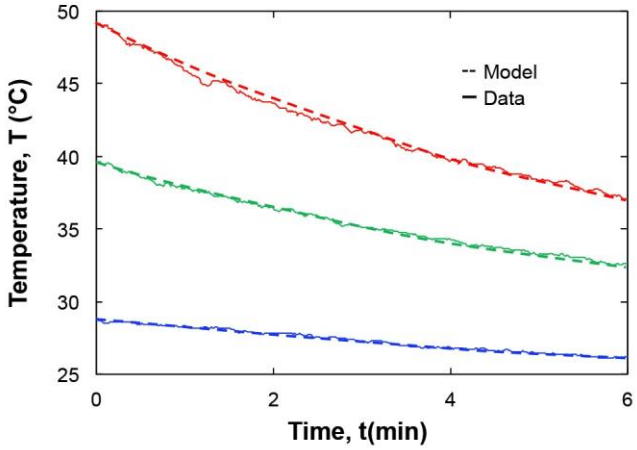

Figure B2. Water surface temperature as a function of time over three initial temperatures (29 ºC, 40 ºC, 49 ºC) measured using infrared thermography.

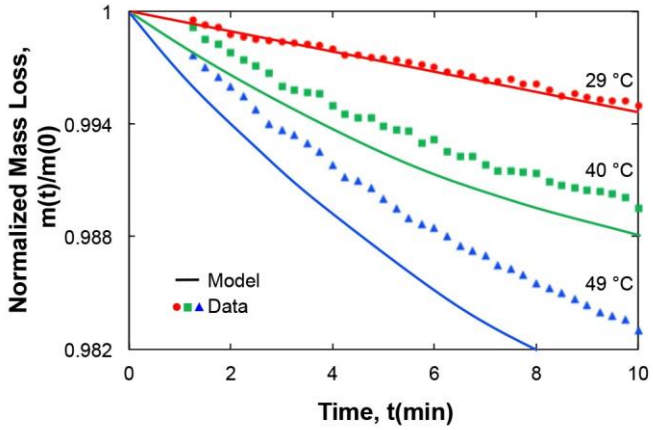

Figure B3. Dimensionless mass loss (closed symbols) measured as a function of time by gravimetric analysis. Solid lines reflect theory in Appendix B corresponding to the three initial temperatures in Figure B2.

We desire h_{nat} from measurements reported in Figures B2 and B3. Because the Biot number for water in the apparatus vessel is small (B < 0.1), we write a lumped energy balance including contributions from evaporative cooling and environmental heat loss (natural convection and radiation). Under well-mixed conditions, the measured water surface temperature obeys the following relation

$$m(t)\hat{C}_p \frac{dT}{dt} = -\hat{J}_W(T) A \Delta\hat{H}_{vap} - h_{nat}(T) A[T - T_\infty] - 4\varepsilon\sigma A[T^4 - T_\infty^4] \qquad \text{(B1)}$$

where $m(t)$ is the time-dependent mass of water in the vessel, A is the cross-sectional area of the vessel, and $\hat{J}_W(T)$ is the temperature-dependent pure-water evaporative flux. In Eq. B1, we retain the full nonlinear form of the Stefan-Boltzmann law.[46,49] Likewise, evaporative-water mass loss in the apparatus is governed by the simple expression

$$\frac{dm(t)}{dt} = -\hat{J}_W(T)A \tag{B2}$$

As noted above, the temperature dependence of $\hat{J}_W$ must be included in Eqs. B1 and B2 to quantify the declining rates of mass loss reported in Figure B3. Pure-water evaporation is mass-transfer controlled[25] or

$$\hat{J}_W(T) = k_m(T)\left[\frac{P_w^{sat}(T)}{RT} - R_H\frac{P_w^{sat}(T_\infty)}{RT_\infty}\right] \tag{B3}$$

where $k_m(T)$ is the temperature-dependent mass transfer coefficient, R is the ideal gas constant, R_H is the ambient relative humidity, and $P_w^{sat}(T)$ is the vapor pressure of water described by the Antoine equation

$$\log_{10} P_w^{sat}(\mathrm{T}) = A - \frac{B}{(T+C)} \tag{B4}$$

where $A = 10.33$ Pa, $B = 1643$ Pa-K, and $C = -42.85$ K.[51] To specify the temperature dependence of k_m, we adopt a Sherwood-number correlation for natural convection of water evaporating from a horizontal, circular plate[52-55]

$$Sh(T) = \frac{k_m(T)D}{D_{wa}(T)} = 0.764Sc^{1/3}(T)Ra_D^{0.205}(T) \tag{B5}$$

where D is the diameter of the cylindrical vessel, D_{wa} is the molecular diffusion coefficient of water vapor in air predicted from $D_{wa} = D_{wa}^o(T/T_o)^{3/2}$, and $D_{wa}^o = 2.6x10^{-5}$ m^2/s is the reference diffusion coefficient at temperature T_o (here 30 °C).[52] In Eq. B5, Sc is the Schmidt number

given by $Sc(T) = \nu_a(T) / D^{\circ}_{wa}$ where $\nu_a(T)$ is the temperature-dependent kinematic viscosity of air.[52] The Rayleigh number in Eq. B5 is defined as[46,52]

$$Ra_D = \frac{[\rho_\infty(T_\infty) - \rho(T)]gD^3}{\langle\rho\rangle \nu_a(T)\alpha_a(T)} \tag{B6}$$

$\rho RT = M_w R_H P_w^{sat}(T) + M_a[P_{atm} - R_H P_w^{sat}(T)]$, $\langle\rho\rangle = (\rho_\infty + \rho)/2$, $\alpha_a(T)$ is the thermal diffusivity of air, g is gravitational acceleration, P_{atm} is atmospheric pressure, and M_w and M_a are the molar masses of water and dry air, respectively. Eqs. B3 – B6 establish the temperature dependence of the water evaporation rate.

In similar fashion, the temperature dependence of h_{nat} follows from a Nusselt-number correlation for a horizontal plate under free convection.[54,55]

$$Nu(T) = \frac{h_{nat}(T)L}{k_a(T)} = 0.54 Ra_L^{1/4}(T) \tag{B7}$$

where the characteristic length $L = D/4$ is the ratio of surface area to perimeter of the circular vessel, $k_a(T)$ is the thermal conductivity of air, and $Ra(T)$ is defined as above.

The 30 °C data in Figures B2 and B3 reveal only a small surface temperature decline and an almost linear decline in mass. Eqs. B1–B4 are solved numerically by a Runge-Kutta algorithm with k_m and h_{nat} as best-fit constants. Solid lines in Figures B2 and B3 at 30 °C give $k_m(30) = 0.0057$ m/s, $h_{nat}(30) = 13.5$ W/m^2/K, and sets T_o = 325 K. Even though k_m is constant, the evaporation rate still varies with temperature due to the temperature dependence of the bracketed term in Eq. B3. For the remaining initial temperatures (40 and 49 °C in Figures B2

and B3), we also take k_m and h_{nat} as constant, but predict their values for the differing initial temperatures according to Eqs. B5 and B7

$$\frac{k_m(T)}{k_m(T_o)} = \frac{D_{wa}(T)}{D_{wa}(T_o)} \frac{Sh(T)}{Sh(T_o)} \quad \text{and} \quad \frac{h_{nat}(T)}{h_{nat}(T_o)} = \frac{k_a(T)}{k_a(T_o)} \frac{Nu(T)}{Nu(T_o)} \quad \text{for } T = 335, 344 \text{ K} \qquad \text{(B8)}$$

Resulting values are listed in Table B1 after adding h_{rad} = 6 W/m^2/K to h_{nat} to obtain the effective heat transfer coefficient, h_{eff}.

Table B1. Measured (*) and predicted heat and mass transfer coefficients.**

T [°C]	h_{eff} [W/m^2/K]	k_m [m/s]
29	20 (*)	0.0057 (*)
40	23	0.0073
49	24	0.0084

** T, h_{eff}, and k_m are the absolute temperature, effective heat transfer coefficient, and mass transfer coefficient, respectively.

With values of k_m and h_{nat} now known at 40 °C and 49 °C, Eqs. B1 – B4 are solved numerically. Solid lines in Figures B2 and B3 give the result. Predictions agree well for transient water-surface temperatures. Disparities, however, arise between the a priori theory and mass-loss data for the two higher temperatures. Apparently, Eq. B8 underestimates the temperature dependence of k_m. Fortunately, because typical ocular-surface temperatures lie below 40 ºC, the obtained values of k_m and h_{nat} at 29 °C (row one in Table B1) are reasonable for use in the in-vivo model of the text.

REFERENCES ONLY APPEARING IN APPENDIX B

49. Incropera FP, DeWitt DP. Introduction to Heat Transfer, 4th ed. New York: Wiley; 2002.

50. Incropera FP, DeWitt DP. Fundamentals of Heat and Mass Transfer, 5th ed. New York: J. Wiley; 2002.

51. Thomson GW. The Antoine Equation for Vapor-Pressure Data. Chem Rev 1946;38:1–39.

52. Bower SM, Saylor JR. A Study of the Sherwood-Rayleigh Relation for Water Undergoing Natural Convection-Driven Evaporation. Int J Heat Mass Transf 2009;52:3055–63.

53. Vynnycky M, Maeno N. Axisymmetric Natural Convection-Driven Evaporation of Water: Analysis and Numerical Solution. Int J Heat Mass Transf 2012;55: 6238–49.

54. Goldstein RJ, Sparrow EM, Jones DC. Natural Convection Mass Transfer Adjacent to Horizontal Plates. Int J Heat Mass Transf 1973;16:1025–35.

55. Sparrow EM, Kratz GK, Schuerger MJ. Evaporation of Water from a Horizontal Surface by Natural-Convection. J Heat Trans-T ASME 1983;105:469–75.